Superconductivity and Pronounced Electron-Phonon Coupling in Rock-Salt Al_{1-x}O_{1-x} and Ti_{1-x}O_{1-x}

Pjotrs Žguns¹, Nuh Gedik², Bilge Yildiz^{1,3,*} and Ju Li^{1,3,*}

*To whom correspondence should be addressed: byildiz@mit.edu, liju@mit.edu

The highest known ambient-pressure T_c among binary compounds is 40 K (MgB₂). Higher T_c was achieved via the high-pressure route (hydrides) or by adding more elements to the structure (quaternary cuprates, pnictides, etc.). Here, we explore alternative means to achieve high T_c , within binary compounds, by considering "exotic", metastable phases that may emerge under extremely low or high oxygen partial pressure, P_{O2} . To this end, we explore AlO, ScO, TiO, and NbO in the rock-salt (B1) phase, which is known to promote superconductivity. The rock-salt structure of these compounds is thermodynamically unstable, and Al₁O₁, Ti₁O₁, Nb₁O₁ are also latticedynamically unstable. We achieve dynamical stability by introducing metal and oxygen vacancies in the fashion of the NbO-type structure, i.e., $Nb_{1-x}O_{1-x}$ ($x = \frac{1}{4}$). First-principles methods with Wannier interpolation are used to compute electron-phonon coupling, Eliashberg spectral function, and T_c according to the Allen-Dynes equation. The electron-phonon coupling strength, λ , is particularly large in Al_{1-x}O_{1-x} ($\lambda = 2.1$) and Ti_{1-x}O_{1-x} ($\lambda = 1.8$), with T_c of about 35 K at $x = \frac{1}{4}$. Remarkably, the strength of coupling is comparable to that in high-pressure hydrides, yet, in contrast to hydrides and MgB₂, the coupling is largely driven by low-frequency, acoustic phonons. $Sc_{1-x}O_{1-x}$ and $Nb_{1-x}O_{1-x}$ show significantly smaller λ (<0.5) and T_c (<3 K). Further, we investigate hydrogen intercalation as a means to increase λ and T_c . Intercalated $Ti_{1-x}O_{1-x}$ and $Nb_{1-x}O_{1-x}$ are dynamically stable; in these oxides, hydrogen intercalation shifts the Fermi level up, reducing the complexity of the Fermi surface and decreasing λ and T_c in $Ti_{1-x}O_{1-x}$. In $Nb_{1-x}O_{1-x}$, the Fermi level shift is more beneficial, resulting in increasing λ and T_c . In these metallic oxides, H forms hydride ions and contributes to high-frequency modes, increasing the ω_{\log} prefactor of T_c . However, the main contribution to T_c comes from the coupling strength λ . Altogether, our study suggests that metal sub-oxides are promising compounds to achieve strong electron-phonon coupling at ambient pressure, and T_c comparable to that of MgB₂.

1. Introduction

Superconductors are used in key technologies such as strong magnets for medical imaging and maglev trains, the lossless transmission of electricity, quantum computing, etc. Attaining high critical temperature T_c is desirable to bring operation conditions closer to ambient and reduce cooling costs.

Department of Materials Science and Engineering, Massachusetts Institute of Technology, 77 Massachusetts Avenue, Cambridge, MA 02139-4307, USA

² Department of Physics, 77 Massachusetts Avenue, Cambridge, MA 02139-4307, USA

Department of Nuclear Science and Engineering, Massachusetts Institute of Technology, 77 Massachusetts Avenue, Cambridge, MA 02139-4307, USA

The T_c had long been considered to have an upper bound of about 20 K (the so-called Matthias limit [1,2], and also Cohen–Anderson limit [3,4]), with Nb₃Ge alloy holding the record $T_c \sim 23$ K [5,6] until the discovery of unconventional cuprate superconductors with $T_c \sim 30$ K in 1986 [7] that then grew to ~130 K by 1993 [8]. However, conventional superconductors, those obeying the Bardeen–Cooper–Schrieffer (BCS) theory [9], were mostly within the expected limit. The discovery of MgB₂ conventional superconductor with $T_c \sim 39$ K (2001) [10] sparked enthusiasm to find materials with a higher T_c among the BCS superconductors.

In contrast to unconventional superconductors, the strategies to achieve high T_c in the BCS superconductors are generally well understood. The pioneering work of Ashcroft [11,12] suggested employing exotic (far from ambient) conditions such as extreme pressure, to achieve the metallic phase of hydrogen [11] and metal hydrides [12] where T_c would be driven by high-frequency phonons of the light element and strong electron-phonon (e-ph) coupling. Recent developments of crystal structure prediction algorithms and first-principles calculations of e-ph coupling allowed the identification of superconducting phases and prediction of their T_c , most notably predicting H₃S [13,14] and LaH₁₀ [15,16], with their superconducting properties and T_c s on the order of 200 K confirmed experimentally [17,18].

Superconducting phases may also be promoted by exotic chemical conditions such as the increased chemical potential of species (e.g., exceptionally high or low oxygen partial pressure P_{O2} or gas atmosphere different from ambient). Recently, Palnichenko and co-workers reported superconducting-like behavior in various metal-oxygen systems such as Na/NaO_x [19], Mg/MgO_x [20], Al/AlO_x [21], Fe/FeO_x [22], Cu/CuO_x [23], Mo/MoO_{3-x} [24], Bi/Bi₂O₃ [25]. These systems were often obtained by high-temperature oxidation of metals or reduction of oxides, and although superconductivity was often volatile and filamentary, the reported $T_{\rm c}$ was high, typically on the order of 50 K or even up to 120 K (Fe/FeO_x [22]). Superconducting behavior was also reported in the Bi₂O₃-based memristor device with Bi filaments [26]. In all these examples, metal-oxygen phases or stoichiometries far from conventional may emerge, potentially giving rise a high T_c . Meta-stable compounds were long anticipated to deliver high- T_c superconductivity [5], and these experimental findings motivate us to search among the metaloxygen phases. Identifying such compounds can help us eventually stabilize or synthesize them by means of ampoule or vacuum furnace-based crystal growth [27], or far-from-equilibrium techniques such as plasma treatment [28], or epitaxial film growth [29–31] with lattice-matching substrates, which may be more feasible than applying extreme pressure.

In this work, we search for meta-stable compounds that may emerge under extremely reducing or oxidizing conditions and exhibit high T_c . Since there are many plausible phases of metal oxides, we start with the structure types that are known to promote superconductivity in a variety of chemistries and evaluate their T_c in the BCS framework. One such archetypal structure is the rock-salt structure (B1, Fig. 1a), and several transition metal nitrides and carbides were reported to have a high T_c up to 20–30 K [32,33]. Therefore, we consider the metal oxides in the B1 phase to find out if they could have a strong e-ph coupling and a high T_c . We are further motivated by the fact that $T_c = 5$ K was recently reported in LaO rock-salt oxide [30], and 5.5 K [27] and 7.4 K [29] in TiO were reported recently after improvements in the synthesis procedures, which leaves room for

achieving high T_c in this class of sub-oxide compounds where the metal cation valence is lower than their typical values on the surface of Earth.

Particularly, we explore rock-salt AlO, ScO, TiO, and NbO intermetallic compounds. These oxides have metallic electronic structures (see, e.g., the Materials Project database [34]), allowing us to predict their T_c within the BCS framework. Recently, the T_c of metallic LaO was determined within the BCS framework [35], matching well with the experimental records [30], which is reassuring for our approach. Moreover, Sc, Ti and Nb sequence allows us to explore the periodic trend (we substitute V for Nb since VO has a band gap [34,36]). The ideal, vacancy-free structure of these oxides is thermodynamically and dynamically unstable (i.e., possesses imaginary frequency and is not stable with respect to lattice vibrations). $Ti_{1-x}O_{1-x}$ has vacancies (x = 0.15) that stabilize the structure; Al_{1-x}O_{1-x} is reported for high temperature only [37]; NbO oxide has 25% of vacancies on both oxygen and metal sites, i.e., Nb_{1-x}O_{1-x} ($x = \frac{1}{4}$) [38]. We chose to study these compounds in the form of NbO-type structure (see Fig. 1b), which remedies phononic instabilities and makes these compounds dynamically stable. For the chosen oxides, we perform electronic structure and lattice dynamics calculations, confirming that these compounds are metallic in their normal state and are dynamically stable. We carry out e-ph calculations and employ Wannier interpolation techniques to accurately compute Eliashberg spectral function and e-ph coupling strength, and T_c . Next, we consider the effect of H intercalation and its effect on the electronic structure, dynamics, and e-ph coupling, and T_c . We find that these binary oxides with NbO-type structure can manifest strong e-ph coupling, as observed for Al_{1-x}O_{1-x} ($\lambda = 2.1$) and Ti_{1-x}O_{1-x} ($\lambda = 1.8$). The strength of eph coupling is comparable to that reported for high-pressure, high- T_c hydrides, and is driven primarily by acoustic phonons which now all have positive stiffness. The resultant T_c reaches up to 36 K and is higher than that reported [32,33] in rock-salt nitrides and carbides.

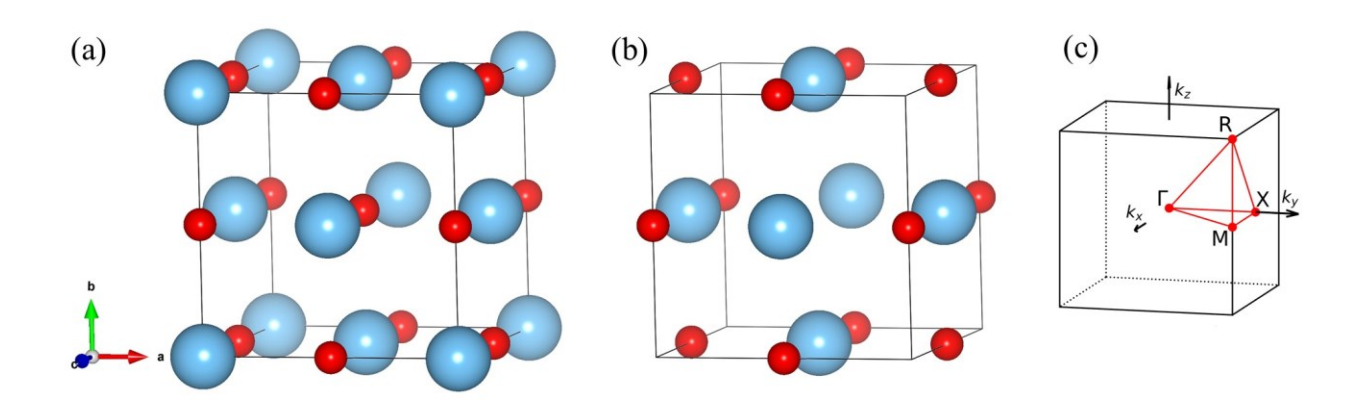


Fig. 1. (a) Conventional unit cell of rock-salt (B1) structure M_1O_1 (cP8, Fm-3m). (b) Conventional unit cell of $M_{1-x}O_{1-x}$ ($x = \frac{1}{4}$, cP6, Pm-3m). It can be seen as a B1 structure with two vacancies at (0, 0, 0) and ($\frac{1}{2}$, $\frac{1}{2}$) sites, as known for NbO [38]. (c) Brillouin zone of the cP unit cell; high-symmetry paths are shown in red. Color code for atoms in (a) and (b): M is blue, O is red.

2. Results and Discussion

 T_c is calculated by following the Allen–Dynes equation with modified $f_{\omega}f_{\mu}$ prefactors that correct predictions for high T_c superconductors [39]:

$$T^{\text{ML}}_{\text{C}} = \frac{f_{\omega} f_{\mu} \omega_{\log}}{1.20} \exp\left(-\frac{1.04(1+\lambda)}{\lambda - \mu^* (1+0.62\lambda)}\right) \tag{1}$$

 μ^* was set to 0.10 in our results. We note there are three factors in equation (1): the exponential factor $\exp\left(-\frac{1.04(1+\lambda)}{\lambda-\mu^*(1+0.62\lambda)}\right)$ that depends on electron-phonon coupling strength λ , the ω_{\log} prefactor, and the $f_{\omega}f_{\mu}$ prefactor (see Methods for the definition of these parameters).

2.1 Al_{1-x}O_{1-x}, Sc_{1-x}O_{1-x}, Ti_{1-x}O_{1-x}, Nb_{1-x}O_{1-x}

Rock-salt Al₁O₁, Sc₁O₁, Ti₁O₁, and Nb₁O₁ compounds are thermodynamically unstable. Their convex hull energies, E_{hull} , range from 0.1 eV/atom to 1.3 eV/atom (see the Materials Project [34,40] data provided in Table S1). Moreover, our phonon calculations show that three of these compounds are dynamically unstable (Al₁O₁, Ti₁O₁, Nb₁O₁). This is expected since Al monoxide is unstable at room temperature [37], while Ti monoxide possesses about 15% of (disordered) Ti and O vacancies (Ti_{0.85}O_{0.85}) [41–43], and Nb monoxide possesses 25% of ordered vacancies (Nb_{0.75}O_{0.75}) [38]. Likewise, theoretical studies of Ti₁O₁ report the appearance of imaginary phonons that can be cured by the introduction of Ti and O vacancies [44]. We show that the introduction of vacancies in the fashion of the NbO-type structure ($x = \frac{1}{4}$) [38] makes Al, Ti, and Nb monoxides significantly more stable, with E_{hull} decreasing by 0.2...0.8 eV/atom (see Table S1; though, only Nb_{0.75}O_{0.75} is thermodynamically stable). Most importantly, all four oxides are dynamically stable in the NbO-type structure, and we therefore used it in further calculations.

Band structure calculations show that $Al_{1-x}O_{1-x}$, $Sc_{1-x}O_{1-x}$, $Ti_{1-x}O_{1-x}$, and $Nb_{1-x}O_{1-x}$ are metallic (Fig. 2a), which agrees with the experimental report of metallic conduction in Ti and Nb monoxides [43]. In $Al_{1-x}O_{1-x}$, the valence band at the Fermi level is dominated by Al 3p and 3s states, with the contribution of O 2p and 2s states (Fig. 2b). In $Sc_{1-x}O_{1-x}$, $Ti_{1-x}O_{1-x}$ and $Nb_{1-x}O_{1-x}$, the Fermi level is dominated by d states, with only marginal contribution of O 2p and other states (Fig. 2b). Electron localization function [45] analysis suggest that these oxides have metallic bonding character especially in between the sites (Fig. 2c), with some strong localization of electrons close to Ti in $Ti_{1-x}O_{1-x}$ and in the oxygen vacancy in $Sc_{1-x}O_{1-x}$ (Fig. 2c).

All four oxides are dynamically stable in the NbO-type phase, as mentioned above; no imaginary frequencies are present (Fig. 3). However, phonon softening is seen in the dispersion: Thus, Al_{1-x}O_{1-x} has significant softening of acoustic modes along the Γ -X and Γ -M paths, indicating proximity to dynamical instability. Indeed, this phase is highly unstable ($E_{\text{hull}} = 0.768 \text{ eV/atom}$, Table S1). These acoustic branches (Γ -X and Γ -M) also show remarkable e-ph coupling as highlighted in Fig. 3a (see Fig. S1 for visualization of these modes). Anomalies such as dispersion wiggles are further seen at different frequency ranges, e.g., around 25–40 meV along the M-R- Γ paths, contributing to the strong e-ph coupling (Fig. 3a). In Ti_{1-x}O_{1-x}, the Γ -X and Γ -M acoustic branches are unusually straight. The strong e-ph coupling can be seen in Fig. 3c for acoustic modes

near the R and M points (see Fig. S2 for visualization of these modes; these modes are octahedral rotations, well-known for the Pm-3m compounds with perovskite-like structure [46,47]; here, octahedra are Ti_6 units).

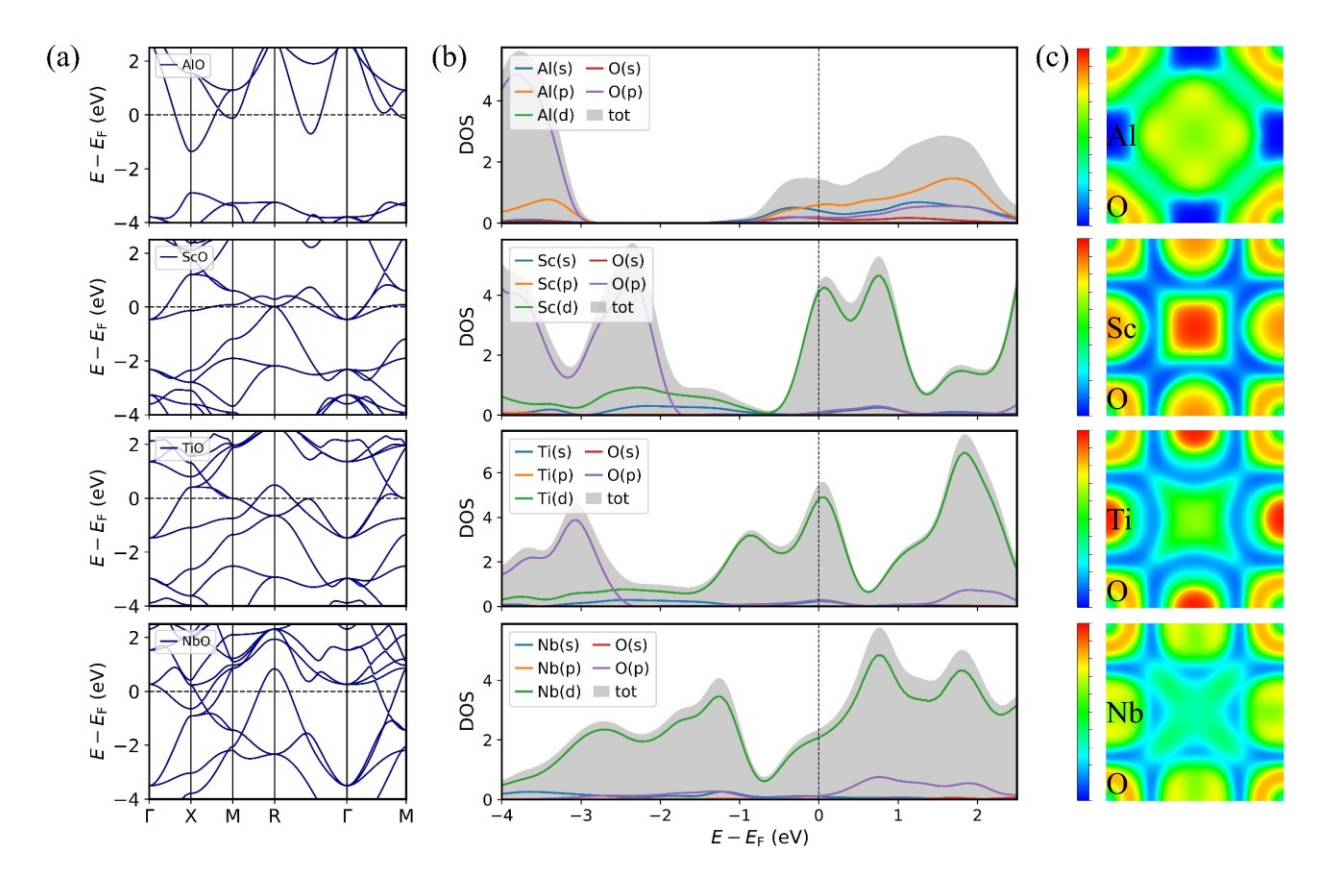


Fig. 2. Electronic structure of $Al_{1-x}O_{1-x}$, $Sc_{1-x}O_{1-x}$, $Ti_{1-x}O_{1-x}$, $Nb_{1-x}O_{1-x}$ ($x = \frac{1}{4}$, cP6, NbO-type structure): (a) Band structure. (b) Projected DOS. (c) Electron localization function colormap of the [002] plane (the vacant oxygen site is in the center). The colormap spans values from 0 (blue) to 1 (red), indicating delocalization and strong localization, respectively. E_F is the Fermi level.

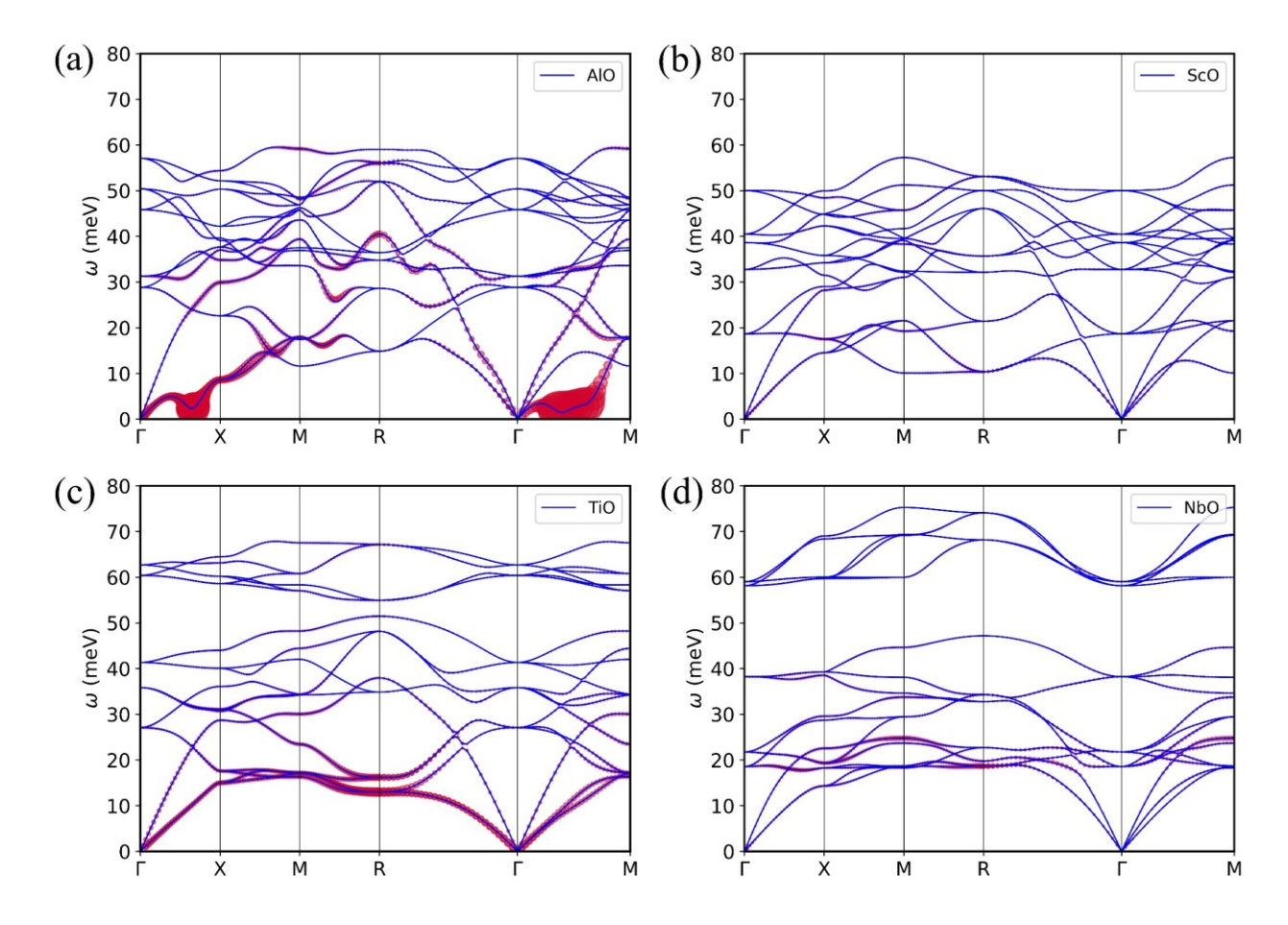


Fig. 3. Phonon dispersion of (a) $Al_{1-x}O_{1-x}$, (b) $Sc_{1-x}O_{1-x}$, (c) $Ti_{1-x}O_{1-x}$, (d) $Nb_{1-x}O_{1-x}$. ($x = \frac{1}{4}$, cP6, NbO-type structure.) All compounds are dynamically stable. The e-ph coupling strength of each mode and q-point (λ_{qv}) is shown with red, filled circles (circle size is proportional to λ_{qv}).

The Eliashberg spectral function and integrated electron-phonon (e-ph) coupling strength, $\lambda(\omega)$, are shown in Fig. 4. In Al_{1-x}O_{1-x}, $\lambda(\omega)$ shows a steady increase and the strongest contribution comes from modes below 35 meV, with a high peak in $\alpha^2 F$ around 32 meV. Acoustic modes extend up to about 25 meV and contribute to λ throughout their frequency range. This agrees with the fact that Al_{1-x}O_{1-x} has phonon anomalies of both acoustic and higher frequency modes. The integrated coupling strength is remarkably high ($\lambda = 2.09$). In Sc_{1-x}O_{1-x}, the e-ph coupling comes from all over the frequency range, however, the coupling is weak ($\lambda = 0.29$). In Ti_{1-x}O_{1-x}, the e-ph coupling is mainly driven by acoustic modes in the 10...20 meV frequency range, which constitutes about 60% of λ . The integrated coupling is strong ($\lambda = 1.80$) and is comparable to that of Al_{1-x}O_{1-x}. In Nb_{1-x}O_{1-x}, the main contribution to λ comes from 15...25 meV acoustic phonons, however, the coupling ($\lambda = 0.47$) is weaker than that in Ti_{1-x}O_{1-x}. Although Sc, Ti and Nb oxides have similar electronic structures, i.e., the Fermi level is dominated by d states, the λ and respective T_c are different. This can be attributed to different electron count, which is an important factor for e-ph coupling. Indeed, the oscillatory variation of T_c along the d elements (Sc, Ti, Nb) is generally consistent with what is known for other superconductors: Thus, T_c shows oscillatory behavior with

the number of valence electrons per atom in various intermetallic compounds and alloys [48–50], as well as rock-salt transition metal carbides and nitrides as reported theoretically [51]. The electron count influences the number of bands and pockets near the Fermi level that can enhance coupling: For example, in $Ti_{1-x}O_{1-x}$, there is a nearly flat band at the Fermi level near the M point and a pocket at the Γ -M path. Furthermore, the absence of strong e-ph coupling in $Sc_{1-x}O_{1-x}$, which also have nearly flat bands close to the Fermi level, may be attributed to charge localization at the O vacancy site, as observed for only this compound (see Bader charges in Table S2 and strong localization at the vacancy site in Fig. 2c). The charge localized at the interstitial sites is known to couple weakly with phonons and is therefore detrimental for the e-ph coupling as reported for high-pressure Li-S compounds [52].

The summary of calculated λ and T_c is shown in Table 1. Intriguingly, $Al_{1-x}O_{1-x}$ and $Ti_{1-x}O_{1-x}$ show pronounced coupling ($\lambda \approx 2$), and T_c on the order of 35 K, which is relatively high for binary compounds at ambient pressure. For example, MgB₂ [53] and related Li-Mg-B superconductors [54] have λ of 0.5–0.7, with the main contribution to coupling originating from high-frequency modes of Boron atoms (above 50 meV). Strong coupling on the order of $\lambda \sim 2$ was reported in high-pressure, high- T_c hydrides such as LaH₁₀ ($\lambda = 2.2$ at 250 GPa) and YH₁₀ ($\lambda = 2.6$ at 250 GPa) [15], as well as H₃S ($\lambda = 2.6$ at 200 GPa) [55], and more recently in ambient-pressure meta-stable Mg₂IrH₆ ($\lambda = 2.5$ at ambient pressure) [56]. However, in H₃S it originates mainly from high-frequency H modes (above 50 meV) [55]. In contrast, the strong e-ph coupling in Al_{1-x}O_{1-x} and Ti_{1-x}O_{1-x} comes from mainly acoustic and low-frequency phonons (below 35 meV, Figs. 3 and 4), dominated by the metal cation participation (especially for Ti_{1-x}O_{1-x}, see Fig. S3). A strong e-ph coupling originating from low-frequency modes was recently reported in PdCuH_x [57], and rock-salt transition metal carbides, namely VC, CrC, MnC and ZnC [33], however the resultant T_c was somewhat smaller (up to 28 K in ZnC).

Few words should be said about the comparison with the available experimental and theoretical data. First, Nb_{0.75}O_{0.75} is a well-known superconductor with a $T_c = 1.4$ K [43], which is reasonably reproduced in our calculations ($T_c = 2.8 \text{ K}$). The T_c of $Al_{1-x}O_{1-x}$ is not known experimentally, since this compound was reported only at elevated temperatures to date [37]. For $Ti_{1-x}O_{1-x}$, the following T_c values were reported: 0.6 K [43], 1.4 K [58], 0.7–2.3 K [59], and even 5.5 K [27] and 7.4 K [29] more recently. The disorder of vacancies was considered one of the plausible sources for decreasing T_c in Ti monoxide [43], which also increases the resistance of the normal, metallic state. Previous theoretical work on TiO ($x = \frac{1}{8}$) has found much smaller $\lambda = 0.8$ and $T_c = 7$ K [44], however the discrepancy might be attributed to different compositions and/or insufficient sampling of k and q points in the ref. [44]. Our calculated T_c , of $Ti_{1-x}O_{1-x}$ is, however, much greater (35 K) than that previously reported in experiments. The difference can be attributed to a different composition ($x = \frac{1}{4}$ in our work vs. x = 0.15 in experiments [41,42]). Further, accounting for plausible anharmonic effects may decrease the calculated T_c, as reported for AlH₃ [60] and YH₆ [61]. Magnetic order may also decrease the T_c [33], which might be relevant for $Ti_{1-x}O_{1-x}$ that has slight ferromagnetic magnetization according to the MP database [34,40]. Electron correlation effects may also influence the T_c of oxides as demonstrated for bismuthate superconductors [62].

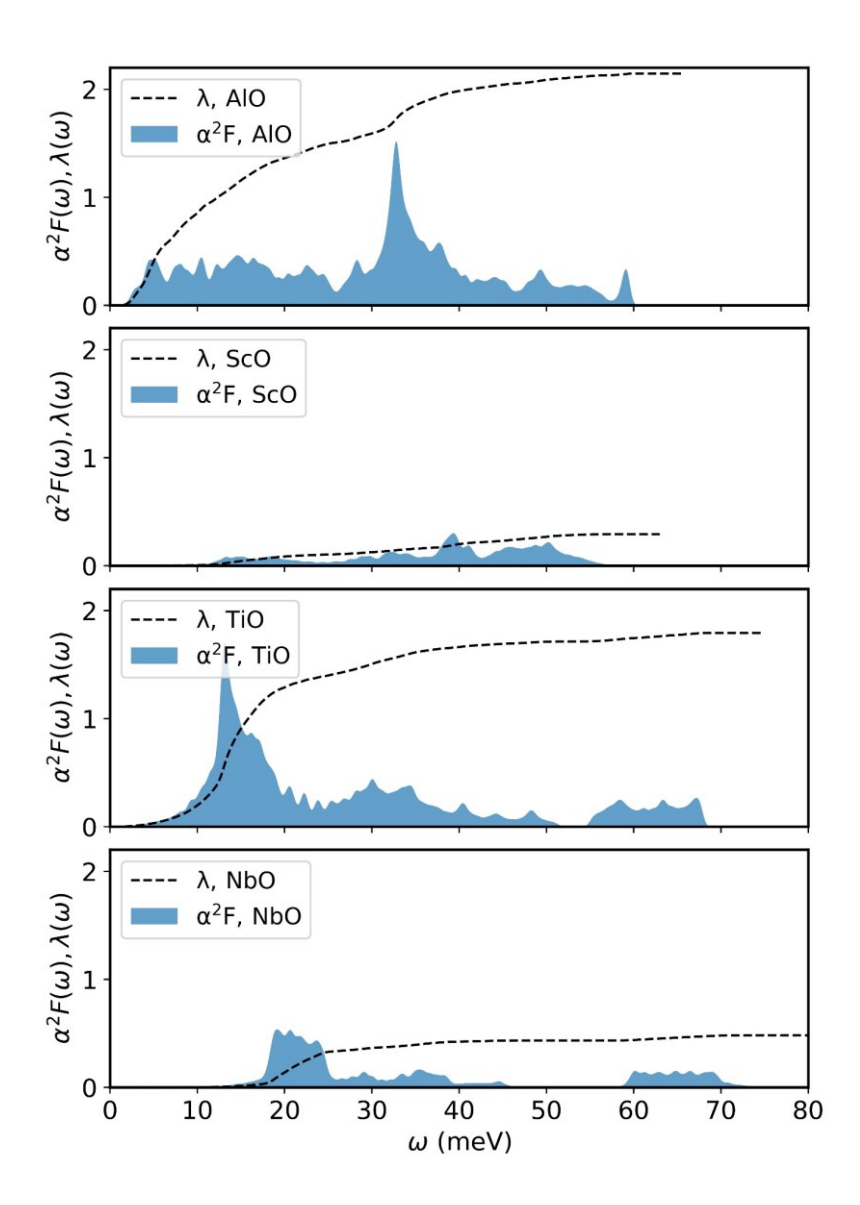


Fig. 4. Eliashberg spectral function $\alpha^2 F(\omega)$ and $\lambda(\omega)$ of Al_{1-x}O_{1-x}, Sc_{1-x}O_{1-x}, Ti_{1-x}O_{1-x}, and Nb_{1-x}O_{1-x} ($x = \frac{1}{4}$, cP6, NbO-type structure).

Table 1. λ , ω_{log} , and T_c^{ML} of Al_{1-x}O_{1-x}, Sc_{1-x}O_{1-x}, Ti_{1-x}O_{1-x} and Nb_{1-x}O_{1-x} oxides ($x = \frac{1}{4}$, NbO-type structure).

Compound	$\omega_{\log} ({\rm meV})$	λ	$T_{\rm c}^{\rm ML}\left({\rm K}\right)$
$Al_{1-x}O_{1-x}$	13.3	2.09	36
$Sc_{1-x}O_{1-x}$	0.1	0.29	0.1
$Ti_{1-x}O_{1-x}$	16.8	1.80	35
$Nb_{1-x}O_{1-x}$	25.4	0.47	2.8

Noteworthy, achieving a high T_c in the BCS superconductors depends on both the strong e-ph coupling and the ω_{log} prefactor (according to the Allen-Dynes formula [39,63]). For example, a twofold increase of λ alone in Al_{1-x}O_{1-x} would increase T_c by 37%; a two-fold increase of ω_{log} alone would increase T_c by 100% (this estimate is oversimplified since λ and ω_{log} are interdependent).

To increase λ and ω_{\log} , the introduction of H, which has a low atomic mass and high vibrational frequency, may be helpful. We therefore study it in the next section to see if it can enhance T_c through both λ and ω_{\log} factors in equation (1) (for details, see Methods).

2.2 Hydrogenated oxides: Ti_{1-x}(O_{1-x}H_x), Nb_{1-x}(O_{1-x}H_x)

Intercalation of hydrogen in oxides with NbO-type structure can occur on either the metal or oxygen vacancy site ($x = \frac{1}{4}$). Our calculations show that intercalation into the metal vacancy site is energetically unfavorable (requires about 3 eV per H atom, for $(M_{1-x}H_x)O_{1-x}$, $x = \frac{1}{4}$), and the obtained structures are dynamically unstable. Intercalation into the oxygen vacancy site is unfavorable for $Al_{1-x}O_{1-x}$ (1.3 eV per H atom), and favorable for $Sc_{1-x}O_{1-x}$, $Ti_{1-x}O_{1-x}$ and $Nb_{1-x}O_{1-x}$ (-0.2 eV to -0.8 eV per H, see Table S3). However, $Sc_{1-x}(O_{1-x}H_x)$ is dynamically unstable, while $Ti_{1-x}(O_{1-x}H_x)$ and $Nb_{1-x}(O_{1-x}H_x)$ are dynamically stable, and we therefore investigate these two latter compounds further.

Band structure calculations show that $Ti_{1-x}(O_{1-x}H_x)$ and $Nb_{1-x}(O_{1-x}H_x)$ are metallic (Fig. 5a). Similar to $Ti_{1-x}O_{1-x}$ and $Nb_{1-x}O_{1-x}$, the valence band at the Fermi level is dominated by d states, with only marginal contribution of O 2p and other states (Fig. 5b). Electron localization function [45] analysis suggest that these oxides have metallic bonding character especially in between the sites, with some strong localization of electrons close to H atoms and Ti in $Ti_{1-x}O_{1-x}$ (Fig. 5c). The Bader charge analysis shows that hydrogen charge state is hydride anion ($q_H = -1.81 |e|$ and -1.68 |e| in $Ti_{1-x}(O_{1-x}H_x)$ and $Nb_{1-x}(O_{1-x}H_x)$, respectively) instead of proton cation.

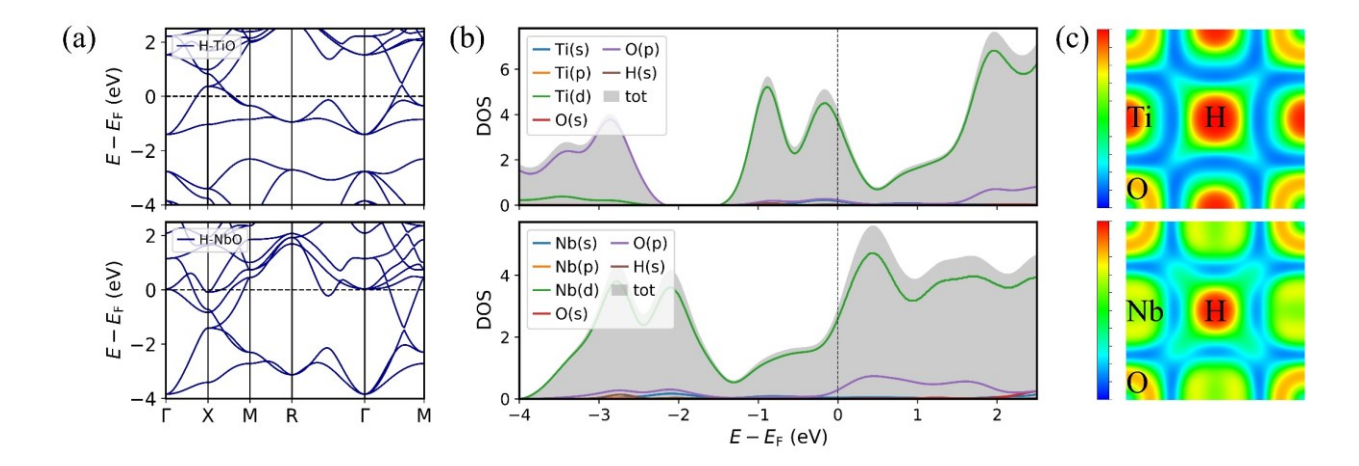


Fig. 5. Electronic structure of $Ti_{1-x}(O_{1-x}H_x)$ and $Nb_{1-x}(O_{1-x}H_x)$: (a) Band structure. (b) Projected DOS. (c) Electron localization function colormap of the [002] plane (hydrogen occupies the vacant oxygen site and is in the center of the colormap). E_F is the Fermi level.

Both $Ti_{1-x}(O_{1-x}H_x)$ and $Nb_{1-x}(O_{1-x}H_x)$ are dynamically stable, as mentioned above; no imaginary frequencies are present (Fig. 6). Some phonon anomalies can be seen in dispersion, e.g., the Γ -X acoustic branches in $Ti_{1-x}(O_{1-x}H_x)$ is unusually straight. The introduction of hydrogen contributes to the formation of high-frequency phonon modes at about 120 meV and 110 meV in $Ti_{1-x}(O_{1-x}H_x)$ and $Nb_{1-x}(O_{1-x}H_x)$, respectively. These phonon modes slightly contribute to e-ph coupling and increase the ω_{log} frequency (from 16.8 meV to 25.7 meV in Ti monoxide, and from 25.4 meV to 27.1 meV in Nb monoxide).

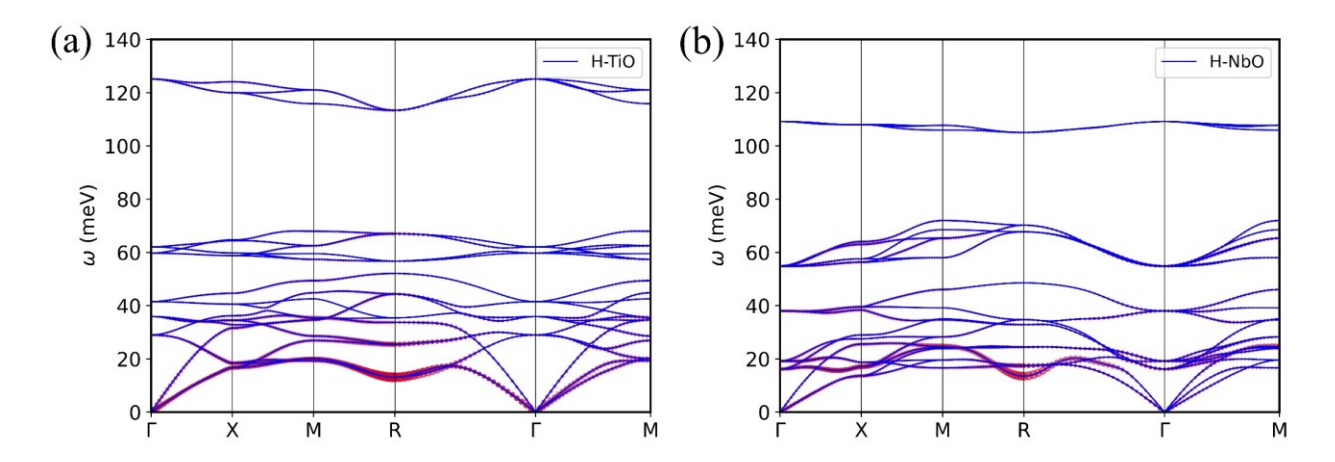


Fig. 6. Phonon dispersion of cP7 (a) $Ti_{1-x}(O_{1-x}H_x)$, (b) $Nb_{1-x}(O_{1-x}H_x)$ ($x = \frac{1}{4}$). Both compounds are dynamically stable (there are no imaginary frequencies). The e-ph coupling strength of each mode and q-point (λ_{qv}) is shown with red, filled circles (circle size is proportional to λ_{qv}).

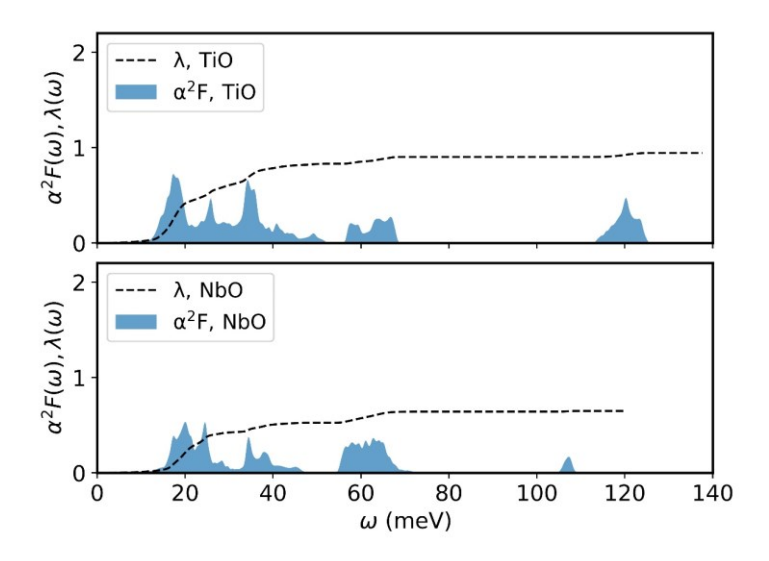


Fig. 7. Eliashberg spectral function $\alpha^2 F(\omega)$ and $\lambda(\omega)$ of cP7 Ti_{1-x}(O_{1-x}H_x) and Nb_{1-x}(O_{1-x}H_x) ($x = \frac{1}{4}$).

Table 2. Electron-phonon coupling, λ , ω_{\log} , $f_{\omega}f_{\mu}/1.20$ prefactor, exponential factor (exp $\{-1.04(1+\lambda)/[\lambda-\mu^*(1+0.62\lambda)]\}$); μ^* was set to 0.10), and critical temperature, T_c^{ML} , of $Ti_{1-x}O_{1-x}$, $Ti_{1-x}(O_{1-x}H_x)$, $Ti_{1-x}O_{1-x}$

Compound	λ	$\omega_{ m log} \ ({ m meV})$	$f_{\omega}f_{\mu}/1.20$ (K/meV)	exp. factor.	$T_{ m c}^{ m ML}$ (K)
$Ti_{1-x}O_{1-x}$ $Ti_{1-x}O_{1-x}H_x$	1.80	16.8	13.0	0.16	35
	(×0.5) 0.96	(×1.5) 25.7	(×0.8) 10.4	(×0.5) 0.08	(×0.6) 21
$Nb_{1-x}O_{1-x} Nb_{1-x}O_{1-x}H_x$	0.47	25.4	9.8	0.011	2.8
	(×1.4) 0.66	(×1.1) 27.1	(×1.0) 9.3	(×3.2) 0.036	(×3.3) 9.1

Significantly, the e-ph coupling in $Ti_{1-x}(O_{1-x}H_x)$ is much decreased as compared to $Ti_{1-x}O_{1-x}$. In $Ti_{1-x}(O_{1-x}H_x)$, the contribution at 10...20 meV is much smaller (Fig. 7). The main origin of this reduction may come from the change in the electronic structure: in $Ti_{1-x}O_{1-x}$ the Fermi level crosses the bands at the Γ -M path and crosses a flat segment near the M point. Intercalation of hydrogen changes the number of valence electrons and shifts these bands below, reducing the complexity of the Fermi surface of $Ti_{1-x}(O_{1-x}H_x)$ as compared to that in $Ti_{1-x}O_{1-x}$ (Fig. 2a and Fig. 5a). In Nb_{1-x}(O_{1-x}H_x), the e-ph coupling is slightly increased as compared to Nb_{1-x}O_{1-x}. In the former compound, the contribution at 60...70 meV is stronger and H also contributes to coupling at 110 meV. H intercalation shifts the Fermi level up and contributes to the complexity of the Fermi surface, where bands at X and Γ points and Γ -R path are closer to the Fermi level, which can promote the coupling.

The analysis of contributions to critical temperature (Table 2) shows that the main contribution to T_c comes from the change in the exponential factor (as one may expect). Although hydrogen intercalation boosts the ω_{\log} frequency, especially in $\text{Ti}_{1-x}(\text{O}_{1-x}H_x)$, the decrease of λ overrides this beneficial effect and T_c of titanium oxide decreases. Altogether, this means that e-ph coupling strengths have the dominant influence on T_c in these oxides.

3. Conclusions

Binary oxides with the NbO-type structure can manifest strong electron-phonon coupling, as observed for $Al_{1-x}O_{1-x}$ ($\lambda = 2.1$) and $Ti_{1-x}O_{1-x}$ ($\lambda = 1.8$) in this work at $x = \frac{1}{4}$. The strength of the eph coupling is comparable to that reported for high-pressure, high- T_c hydrides ($\lambda \approx 2-3$) [15,55]. In $Al_{1-x}O_{1-x}$, the coupling is driven by phonon anomalies at various phonon frequencies. In $Ti_{1-x}O_{1-x}$, the coupling is primarily driven by acoustic phonons. The computationally predicted T_c reaches 36 K for $Al_{1-x}O_{1-x}$ and 35 K for $Ti_{1-x}O_{1-x}$, which is higher than in counterpart nitrides and carbides reported to date, where superconductivity also emerges from phonon mode anomalies [33,51]. The T_c and e-ph coupling are sensitive to the intercalation of hydrogen in the Ti and Nb monoxides, as it changes the number of valence electrons and thus the band structure at the Fermi level.

Altogether, such intermetallic oxides with phonon anomalies are attractive for further investigation to achieve high T_c .

4. Computational Methods

Density functional theory [64,65] calculations were performed with the Quantum Espresso package [66-68]. Perdew-Burke-Ernzerhof exchange-correlation functional [69,70] and normconserving scalar-relativistic pseudopotentials, as provided in the PseudoDojo database (v0.4.1) [71], were employed. Planewave kinetic energy cut-off for wavefunctions was set to 90 Ry. Brillouin zone integration was performed on the Γ-centered 16×16×16 k-mesh (for Sc_{1-x}O₁₋ x, Ti_{1-x}O_{1-x}, Nb_{1-x}O_{1-x}; for Al_{1-x}O_{1-x}, 20×20×20 k-mesh was used). Lattice parameters and atomic positions were optimized until pressure, total energy and forces converged within 0.1 kbar, 10⁻⁵ Ry, and 10^{-4} Ry/Bohr, respectively (equilibrium lattice parameters are provided in Table S4). The EPW code [53,72,73] was used to calculate electron-phonon coupling on the fine grids. The following orbitals were used for Wannier interpolation: sp³ and d for metal atoms and sp³ for oxygen atoms, and s orbitals for vacant sites and hydrogen. Phonon and electron-phonon interactions were evaluated on the coarse 6×6×6 q-grid and 12×12×12 k-grid. Electron-phonon coupling and Eliashberg spectral function $\alpha^2 F(\omega)$ were evaluated on the interpolated, fine 18×18×18 **q**-grid and 36×36×36 **k**-grid (for AlO, 24×24×24 **q**- and 48×48×48 **k**-grids were used). The $T_{\rm c}$ was calculated following the Allen–Dynes equation [63] with modified $f_{\omega}f_{\mu}$ prefactors that corrects predictions for high T_c superconductors [39]: $T_C^{ML} = \frac{f_\omega f_\mu \omega_{\log}}{1.20} \exp\left(-\frac{1.04(1+\lambda)}{\lambda - \mu^*(1+0.62\lambda)}\right)$,

where
$$f_{\omega}=1.92\left(\frac{\lambda+\frac{\omega_{\log}}{\overline{\omega_{2}}}\sqrt[3]{\mu^{*}}}{\sqrt{\lambda}\exp\left(\frac{\omega_{\log}}{\overline{\omega_{2}}}\right)}\right)-0.08$$
, $f_{\mu}=\frac{6.86\exp\left(\frac{\lambda}{\mu^{*}}\right)}{\frac{1}{\lambda}-\mu^{*}-\frac{\omega_{\log}}{\overline{\omega_{2}}}}+1$, $\lambda=2\int_{0}^{\infty}d\omega\alpha^{2}F(\omega)/\omega$, while $\overline{\omega}_{n}=\langle\omega^{n}\rangle^{1/n}$ and $\langle\omega^{n}\rangle=\frac{2}{\lambda}\int d\omega\alpha^{2}F(\omega)\omega^{n-1}$, and $\omega_{\log}=\lim_{n\to 0}\overline{\omega}_{n}=\exp\left(\frac{2}{\lambda}\int_{0}^{\infty}\frac{d\omega}{\omega}\alpha^{2}F(\omega)\ln\omega\right)$ [63]; μ^{*} was set to 0.10. Calculation of T_{c}^{ML} is implemented in the recent versions of the EPW code. Electron localization function [45] and Bader charges [74,75] were calculated with the VASP code [76–81] for earlier optimized structures. VESTA software was used for the visualization of crystal structure and electron localization function 2D colormaps [82].

Supporting Information

Supporting Information is available from the Wiley Online Library.

Acknowledgment

We acknowledge support by NSF DMR-2132647 "EAGER: SUPER: Electrochemical Protonation to Achieve Superconducting Matter". We acknowledge supercomputer resources provided by the Frontera computing project DMR20012 at the Texas Advanced Computing Center. Frontera is made possible by National Science Foundation award OAC-1818253.

Conflict of Interest

The authors declare that they have no conflict of interest.

Keywords

BCS superconductivity; electron-phonon coupling; sub-oxides

References

- [1] B. T. Matthias, Conclusions from Superconducting Molybdenum Technetium Alloys, Rev Mod Phys **33**, (1961).
- [2] T. H. Geballe, B. T. Matthias, J. P. Remeika, A. M. Clogston, V. B. Compton, J. P. Maita, and H. J. Williams, *High Temperature SP-Band Superconductors*, Physics Physique Fizika **2**, (1966).
- [3] P. W. Anderson and M. L. Cohen, Comments on the Maximum Superconducting Transition Temperature, in Career In Theoretical Physics, A (2nd Edition) (2005).
- [4] L. Boeri, Understanding Novel Superconductors with Ab Initio Calculations, in Handbook of Materials Modeling: Applications: Current and Emerging Materials, Second Edition (2020).
- [5] M. R. Beasley and T. H. Geballe, *Superconducting Materials*, Phys Today **37**, (1984).
- [6] J. Muller, A15-Type Superconductors, Reports on Progress in Physics 43, (1980).
- [7] J. G. Bednorz and K. A. Müller, *Possible HighT c Superconductivity in the Ba–La–Cu–O System*, Zeitschrift Für Physik B Condensed Matter 1986 64:2 **64**, 189 (1986).
- [8] A. Schilling, M. Cantoni, J. D. Guo, and H. R. Ott, *Superconductivity above 130 K in the Hg–Ba–Ca–Cu–O System*, Nature 1993 363:6424 **363**, 56 (1993).
- [9] J. Bardeen, L. N. Cooper, and J. R. Schrieffer, *Theory of Superconductivity*, Physical Review **108**, (1957).
- [10] J. Nagamatsu, N. Nakagawa, T. Muranaka, Y. Zenitani, and J. Akimitsu, Superconductivity at 39 K in Magnesium Diboride, Nature 2001 410:6824 **410**, 63 (2001).
- [11] N. W. Ashcroft, *Metallic Hydrogen: A High-Temperature Superconductor?*, Phys Rev Lett **21**, (1968).
- [12] N. W. Ashcroft, *Hydrogen Dominant Metallic Alloys: High Temperature Superconductors?*, Phys Rev Lett **92**, (2004).
- [13] D. Duan, Y. Liu, F. Tian, D. Li, X. Huang, Z. Zhao, H. Yu, B. Liu, W. Tian, and T. Cui, *Pressure-Induced Metallization of Dense (H2S)2H2 with High-Tc Superconductivity*, Sci Rep 4, 6968 (2014).

- [14] D. Duan, X. Huang, F. Tian, D. Li, H. Yu, Y. Liu, Y. Ma, B. Liu, and T. Cui, *Pressure-Induced Decomposition of Solid Hydrogen Sulfide*, Phys Rev B Condens Matter Mater Phys **91**, (2015).
- [15] H. Liu, I. I. Naumov, R. Hoffmann, N. W. Ashcroft, and R. J. Hemley, *Potential High-Tc Superconducting Lanthanum and Yttrium Hydrides at High Pressure*, Proc Natl Acad Sci U S A **114**, (2017).
- [16] F. Peng, Y. Sun, C. J. Pickard, R. J. Needs, Q. Wu, and Y. Ma, *Hydrogen Clathrate Structures in Rare Earth Hydrides at High Pressures: Possible Route to Room-Temperature Superconductivity*, Phys Rev Lett **119**, (2017).
- [17] A. P. Drozdov, M. I. Eremets, I. A. Troyan, V. Ksenofontov, and S. I. Shylin, *Conventional Superconductivity in H2S at 203 K at High Pressures*, Nature (2015).
- [18] A. P. Drozdov et al., Superconductivity at 250 K in Lanthanum Hydride under High Pressures, Nature **569**, (2019).
- [19] N. S. Sidorov, A. V. Palnichenko, and S. S. Khasanov, *Superconductivity in the Metallic-Oxidized Sodium Interface*, Solid State Commun **150**, (2010).
- [20] N. S. Sidorov, A. V. Palnichenko, and S. S. Khasanov, *Superconductivity in the Metallic-Oxidized Magnesium Interface*, Solid State Commun **152**, 443 (2012).
- [21] A. V. Palnichenko, O. M. Vyaselev, A. A. Mazilkin, and S. S. Khasanov, Superconductivity in Al/Al2O3 Interface, Physica C: Superconductivity and Its Applications **525–526**, 65 (2016).
- [22] N. S. Sidorov, A. V. Palnichenko, and I. I. Zver'Kova, *Superconductivity at 125 K in the Metallic–Oxidized Iron Interface*, Journal of Superconductivity and Novel Magnetism 2010 24:5 **24**, 1433 (2010).
- [23] N. S. Sidorov, A. V. Palnichenko, and S. S. Khasanov, *Superconductivity in the Metallic-Oxidized Copper Interface*, Physica C: Superconductivity and Its Applications **471**, (2011).
- [24] A. V. Palnichenko, I. I. Zver'kova, D. V. Shakhrai, and O. M. Vyaselev, *Metastable Superconductivity of Mo/MoO3–x Interface*, Physica C: Superconductivity and Its Applications **558**, 25 (2019).
- [25] A. V. Palnichenko, A. A. Mazilkin, O. G. Rybchenko, D. V. Shakhrai, and O. M. Vyaselev, *Superconducting-like Behavior of Bi/Bi2O3 Interface*, Physica C: Superconductivity and Its Applications **571**, 1353608 (2020).
- [26] J. A. Koza, E. W. Bohannan, and J. A. Switzer, Superconducting Filaments Formed during Nonvolatile Resistance Switching in Electrodeposited δ-Bi2o3, ACS Nano 7, (2013).

- [27] D. Wang, C. Huang, J. He, X. Che, H. Zhang, and F. Huang, *Enhanced Superconductivity in Rock-Salt TiO*, ACS Omega **2**, 1036 (2017).
- [28] G. Xu et al., Self-Perpetuating Carbon Foam Microwave Plasma Conversion of Hydrocarbon Wastes into Useful Fuels and Chemicals, Environ Sci Technol 55, (2021).
- [29] C. Zhang, F. Hao, G. Gao, X. Liu, C. Ma, Y. Lin, Y. Yin, and X. Li, *Enhanced Superconductivity in TiO Epitaxial Thin Films*, NPJ Quantum Mater **2**, (2017).
- [30] K. Kaminaga, D. Oka, T. Hasegawa, and T. Fukumura, *Superconductivity of Rock-Salt Structure LaO Epitaxial Thin Film*, J Am Chem Soc **140**, (2018).
- [31] Y. Li et al., Anomalous Negative Resistance in SrTaO3 Thin Film: The Nonuniform Electronic State with Possible Superconductivity around 40 K, J Appl Phys 134, (2023).
- [32] D. A. Papaconstantopoulos, W. E. Pickett, B. M. Klein, and L. L. Boyer, *Superconductivity: Nitride Offers 30K Transition?*, Nature **308**, (1984).
- [33] N. J. Szymanski, I. Khatri, J. G. Amar, D. Gall, and S. V. Khare, *Unconventional Superconductivity in 3d Rocksalt Transition Metal Carbides*, J Mater Chem C Mater 7, (2019).
- [34] A. Jain et al., Commentary: The Materials Project: A Materials Genome Approach to Accelerating Materials Innovation, APL Mater 1, 011002 (2013).
- [35] P. H. Sun, J. F. Zhang, K. Liu, Q. Han, and Z. Y. Lu, First-Principles Study of the Superconductivity in LaO, Phys Rev B **104**, (2021).
- [36] W. C. Mackrodt, D. S. Middlemiss, and T. G. Owens, *Hybrid Density Functional Theory Study of Vanadium Monoxide*, Phys Rev B Condens Matter Mater Phys **69**, (2004).
- [37] M. Hoch and H. L. Johnston, Formation, Stability and Crystal Structure of the Solid Aluminum Suboxides: A12O and AlO1, J Am Chem Soc 76, (1954).
- [38] G. Andersson, A. Magnéli, K. Marcker, and L. G. Sillén, *Note on the Crystal Structure of Niobium Monoxide.*, Acta Chem Scand **11**, (1957).
- [39] S. R. Xie et al., Machine Learning of Superconducting Critical Temperature from Eliashberg Theory, NPJ Comput Mater 8, (2022).
- [40] Https://Materialsproject.Org/, (unpublished).
- [41] Paul Ehrlich, *Phasenverhältnisse Und Magnetisches Verhalten Im System Titan/Sauerstoff*, Zeitschrift Für Elektrochemie Und Angewandte Physikalische Chemie **45**, 362 (1939).
- [42] S. Andersson, B. Collén, U. Kuylenstierna, A. Magnéli, A. Magnéli, H. Pestmalis, and S. Åsbrink, *Phase Analysis Studies on the Titanium-Oxygen System.*, Acta Chem Scand 11, (1957).

- [43] J. K. Hulm, C. K. Jones, R. A. Hein, and J. W. Gibson, *Superconductivity in the TiO and NbO Systems*, J Low Temp Phys **7**, (1972).
- [44] S. V. Hosseini, M. Abbasnejad, and M. R. Mohammadizadeh, *Electron-Phonon Interaction in Tin O2n-1 Using First-Principles Calculations*, Phys Rev B **104**, 224101 (2021).
- [45] B. Silvi and A. Savin, Classification of Chemical Bonds Based on Topological Analysis of Electron Localization Functions, Nature 371, (1994).
- [46] A. P. Giddy, M. T. Dove, G. S. Pawley, and V. Heine, *The Determination of Rigid-unit Modes as Potential Soft Modes for Displacive Phase Transitions in Framework Crystal Structures*, Acta Crystallographica Section A **49**, (1993).
- [47] B. K. Greve, K. L. Martin, P. L. Lee, P. J. Chupas, K. W. Chapman, and A. P. Wilkinson, *Pronounced Negative Thermal Expansion from a Simple Structure: Cubic ScF3*, J Am Chem Soc 132, (2010).
- [48] B. T. Matthias, Empirical Relation between Superconductivity and the Number of Valence Electrons per Atom, Physical Review 97, (1955).
- [49] W. L. McMillan, *Transition Temperature of Strong-Coupled Superconductors*, Physical Review **167**, 331 (1968).
- [50] E. E. Havinga, H. Damsma, and M. H. Van Maaren, *Oscillatory Dependence of Superconductive Critical Temperature on Number of Valency Electrons in Cu3Au-Type Alloys*, Journal of Physics and Chemistry of Solids **31**, (1970).
- [51] E. I. Isaev, S. I. Simak, I. A. Abrikosov, R. Ahuja, Y. K. Vekilov, M. I. Katsnelson, A. I. Lichtenstein, and B. Johansson, *Phonon Related Properties of Transition Metals, Their Carbides, and Nitrides: A First-Principles Study*, J Appl Phys **101**, (2007).
- [52] C. Kokail, C. Heil, and L. Boeri, Search for High- Tc Conventional Superconductivity at Megabar Pressures in the Lithium-Sulfur System, Phys Rev B **94**, (2016).
- [53] E. R. Margine and F. Giustino, *Anisotropic Migdal-Eliashberg Theory Using Wannier Functions*, Phys Rev B Condens Matter Mater Phys **87**, 024505 (2013).
- [54] G. P. Kafle, C. R. Tomassetti, I. I. Mazin, A. N. Kolmogorov, and E. R. Margine, *Ab Initio Study of Li-Mg-B Superconductors*, Phys Rev Mater **6**, (2022).
- [55] I. Errea, M. Calandra, C. J. Pickard, J. Nelson, R. J. Needs, Y. Li, H. Liu, Y. Zhang, Y. Ma, and F. Mauri, *High-Pressure Hydrogen Sulfide from First Principles: A Strongly Anharmonic Phonon-Mediated Superconductor*, Phys Rev Lett **114**, (2015).
- [56] K. Dolui, L. J. Conway, C. Heil, T. A. Strobel, R. Prasankumar, and C. J. Pickard, Feasible Route to High-Temperature Ambient-Pressure Hydride Superconductivity, Phys. Rev. Lett. 132, 166001 (2024).

- [57] R. Vocaturo, C. Tresca, G. Ghiringhelli, and G. Profeta, *Prediction of Ambient-Pressure Superconductivity in Ternary Hydride PdCuHx*, J Appl Phys **131**, (2022).
- [58] M. D. Banus, T. B. Reed, and A. J. Strauss, *Electrical and Magnetic Properties of TiO and VO*, Phys Rev B **5**, (1972).
- [59] N. J. Doyle, J. K. Hulm, C. K. Jones, R. C. Miller, and A. Taylor, *Vacancies and Superconductivity in Titanium Monoxide*, Phys Lett A **26**, (1968).
- [60] B. Rousseau and A. Bergara, *Giant Anharmonicity Suppresses Superconductivity in AlH3 under Pressure*, Phys Rev B Condens Matter Mater Phys **82**, (2010).
- [61] I. A. Troyan et al., *Anomalous High-Temperature Superconductivity in YH6*, Advanced Materials **33**, (2021).
- [62] Z. P. Yin, A. Kutepov, and G. Kotliar, Correlation-Enhanced Electron-Phonon Coupling: Applications of GW and Screened Hybrid Functional to Bismuthates, Chloronitrides, and Other High-Tc Superconductors, Phys Rev X 3, 021011 (2013).
- [63] P. B. Allen and R. C. Dynes, *Transition Temperature of Strong-Coupled Superconductors Reanalyzed*, Phys Rev B **12**, (1975).
- [64] P. Hohenberg and W. Kohn, *Inhomogeneous Electron Gas*, Physical Review **136**, B864 (1964).
- [65] W. Kohn and L. J. Sham, *Self-Consistent Equations Including Exchange and Correlation Effects*, Physical Review **140**, A1133 (1965).
- [66] P. Giannozzi et al., QUANTUM ESPRESSO: A Modular and Open-Source Software Project for Quantum of Materials, Journal of Physics: Condensed Matter 21, 395502 (2009).
- [67] P. Giannozzi et al., *Advanced Capabilities for Materials Modelling with Quantum ESPRESSO*, Journal of Physics: Condensed Matter **29**, 465901 (2017).
- [68] P. Giannozzi et al., *Quantum ESPRESSO toward the Exascale*, Journal of Chemical Physics **152**, 154105 (2020).
- [69] J. P. Perdew, K. Burke, and M. Ernzerhof, *Generalized Gradient Approximation Made Simple*, Phys Rev Lett **77**, 3865 (1996).
- [70] J. P. Perdew, K. Burke, and M. Ernzerhof, *Erratum: Generalized Gradient Approximation Made Simple (Physical Review Letters (1996) 77 (3865))*, Phys Rev Lett **78**, 1396 (1997).
- [71] M. J. van Setten, M. Giantomassi, E. Bousquet, M. J. Verstraete, D. R. Hamann, X. Gonze, and G. M. Rignanese, *The PseudoDojo: Training and Grading a 85 Element Optimized Norm-Conserving Pseudopotential Table*, Comput Phys Commun **226**, 39 (2018).

- [72] F. Giustino, M. L. Cohen, and S. G. Louie, *Electron-Phonon Interaction Using Wannier Functions*, Phys Rev B Condens Matter Mater Phys **76**, 165108 (2007).
- [73] S. Poncé, E. R. Margine, C. Verdi, and F. Giustino, *EPW: Electron-Phonon Coupling, Transport and Superconducting Properties Using Maximally Localized Wannier Functions*, Comput Phys Commun **209**, 116 (2016).
- [74] R. F. W. Bader, Atoms in Molecules: A Quantum Theory (Clarendon Press, 1990).
- [75] W. Tang, E. Sanville, and G. Henkelman, *A Grid-Based Bader Analysis Algorithm without Lattice Bias*, Journal of Physics Condensed Matter **21**, 7 (2009).
- [76] G. Kresse and J. Furthmüller, *Efficient Iterative Schemes for Ab Initio Total-Energy Calculations Using a Plane-Wave Basis Set*, Phys Rev B Condens Matter Mater Phys **54**, 11169 (1996).
- [77] G. Kresse and J. Furthmüller, Efficiency of Ab-Initio Total Energy Calculations for Metals and Semiconductors Using a Plane-Wave Basis Set, Comput Mater Sci 6, 15 (1996).
- [78] G. Kresse and J. Hafner, *Ab Initio Molecular-Dynamics Simulation of the Liquid-Metalamorphous- Semiconductor Transition in Germanium*, Phys Rev B **49**, 14251 (1994).
- [79] G. Kresse and J. Hafner, *Ab Initio Molecular Dynamics for Liquid Metals*, Phys Rev B **47**, 558 (1993).
- [80] P. E. Blöchl, *Projector Augmented-Wave Method*, Phys Rev B **50**, 17953 (1994).
- [81] D. Joubert, From Ultrasoft Pseudopotentials to the Projector Augmented-Wave Method, Phys Rev B Condens Matter Phys **59**, 1758 (1999).
- [82] K. Momma and F. Izumi, VESTA 3 for Three-Dimensional Visualization of Crystal, Volumetric and Morphology Data, Urn:Issn:0021-8898 44, 1272 (2011).